

Thermo-flow and temperature sensing behaviour of graphene based on surface heat convection

Haider Al-Mumen^{1,2}, Fubo Rao¹, Lixin Dong¹, Wen Li¹

¹Department of Electrical and Computer Engineering, Michigan State University, East Lansing, MI 48824-1226, USA

²Department of Electrical Engineering, University of Babylon, Babylon, Iraq

E-mail: wenli@egr.msu.edu

Published in Micro & Nano Letters; Received on 15th May 2013; Revised on 0th 0000; Accepted on 1st August 2013

This letter studies the surface heat convection of thin graphene sheets and the application of graphene wires as nanoscale flow and temperature sensors. Graphene wires with relatively large length-to-width ratios were designed and fabricated using bi- and few-layer graphene sheets. Prior to testing, the devices were packaged in a microfluidic chamber with capillary tubes as upstream and downstream connections to minimise environmental interference. The thermal inertia of the graphene wire was studied at 70°C and the flow sensing behaviour of the device was characterised by monitoring normalised resistance changes at different flow rates. The authors experimental results demonstrated the negative temperature coefficients of the bi- and few-layer graphene films. Moreover, the flow sensing resolutions of ~ 0.07 l/min and 0.1 l/min were achieved from the bi- and few-layer graphene hot wires, respectively. The temperature sensing behaviour of the graphene thermistor was studied in a small temperature range from room temperature to 80°C. The larger negative temperature coefficient of the bi-layer graphene resulted in a higher sensing response than the few-layer one.

1. Introduction: Micro and nanoscale flow sensors offer tremendous opportunities for detecting flow rates in a wide variety of applications, such as microfluidics and lab-on-a-chip systems. Modern flow sensing technologies can be classified into two basic categories: thermal-based [1–7] and mechanical-deflection-based [8–13] sensors. The thermal-based sensors usually involve a hot wire configuration at the millimeter scale, which is mainly made of materials with positive temperature coefficients (PTCs), such as tungsten or platinum [7]. However, PTC sensors suffer from a self-heating effect and slow response time. The sensing principle of the mechanical-deflection-based sensors relies on either cantilever deflection or lift force [8–10]. Although these devices can achieve fast response and high sensitivity, they are fragile and not mechanically stable. Therefore, improved device design and careful selection of materials are required to maximise sensor sensitivity and sensing range, enhance device reliability and reduce device size suitable for use in micro and nanoscale systems.

To address these challenges, we propose to use graphene as the sensing material of a thermal-based flow sensor. Graphene is well known to have unique properties that make it an excellent choice for thermo-flow and temperature sensing applications [14–16]. Graphene is a one-atom-thick layer of carbon and is arranged in a honeycomb lattice. It has a large surface-to-mass ratio and a higher temperature coefficient of resistance (TCR) than tungsten and platinum, resulting in low thermal inertia and high sensitivity to temperature variation. In addition, the negative temperature coefficient (NTC) of graphene [15, 17] enables the self-protection of graphene sensors and minimises sensing error from current-induced Joule heating. Furthermore, the planar design of the hot-wire sensors is mechanically more stable because it has no suspended elements such as cantilevers. Finally, our proposed graphene sensors can be built using conventional micro and nanofabrication techniques with nanoscale sizes, low power and low cost, and thus can be integrated with microfluidic components to achieve complex system functionality. In this study, we used primarily bi- and few-layer graphene as the building material of the hot wire sensors and secondarily mono-layer graphene because of its relatively lower temperature dependence because of the elevated intrinsic mobility of charge carriers [17, 18]. The subsequent sections describe the

theoretical background, design, fabrication process, packaging and characterisation of the graphene flow and thermistor sensors based on the hot-wire configuration.

2. Heat convection theory: Graphene has an NTC property and its resistance (R) at a certain temperature (T) can be represented by $R(T) = R(0) - (\hbar/e^2)((4TV_0)/(\hbar v^2 E_f \tau_0))$ [17] where \hbar is the Planck constant, e is the charge of an electron, v is the velocity, E_f is the Fermi energy, τ_0 is the backscattering rate from atomically sharp defects in graphene lattice and V_0 is the characteristic interaction constant. Heat conduction in graphite and graphene is achieved by both phonons and electrons but the contribution of electrons is very little because of the strong sp^2 bonds of carbon atoms [19]. Therefore graphene sheet resistance (R_s) is approximately proportional to the number of scattered phonons (n_0), $R_s \propto n_0$ and $n_0 = (1/(e^{\hbar\omega/K_B T} - 1))$, where $\hbar\omega$ is the phonon energy, K_B is the Boltzmann constant and T is the temperature [15]. Since acoustic phonons have small energy ($\hbar\omega < K_B T$), the number of scattered phonons can be approximated as

$$n_0 = \frac{1}{e^{\hbar\omega/K_B T} - 1} \simeq \frac{K_B T}{\hbar\omega}$$

and, therefore $R_s \propto T$. Whereas for optical phonons, $\hbar\omega \simeq K_B T$ so $n_0 = (1/(e^{\hbar\omega/K_B T} - 1))$ and then $R_s \propto (1/(e^{\hbar\omega/K_B T} - 1))$. If graphene is deposited on a SiO_2 substrate, the scattered phonons will be the combination of graphene and SiO_2 phonons. In case of suspended graphene, the scattered phonons will be contributed only by graphene. However, the suspended graphene is not preferable in our study since it has little surface disorder, which makes it less sensitive to temperature variation [20–22]. For this reason, the graphene sensors were designed based on a planar hot-wire configuration.

Theoretically, when a hot wire is heated by an electrical current, the thermal energy generated by the wire is equivalent to the energy loss because of convective heat transfer at thermal equilibrium, $I^2 R_w = A_w (T_w - T_f)h$, where A_w denotes the surface area of the wire, T_w and T_f are the wire and fluid temperatures, respectively, h is the heat transfer coefficient and $I^2 R_w$ resembles the thermal energy stored in the wire plus the heat transfer from the surrounding

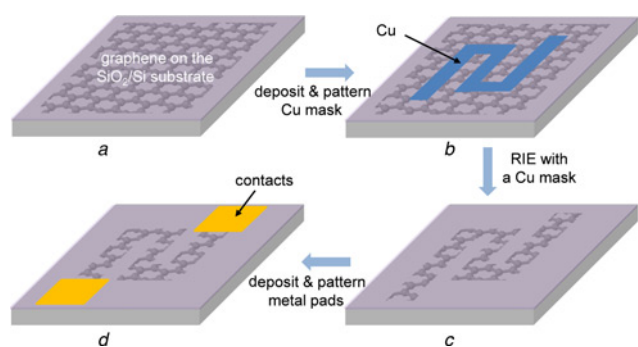


Figure 1 Process flow for making the proposed graphene hot-wire sensors

area. The resistance of the hot wire (R_w) depends on the wire temperature (T_w). At steady state, this resistance can be expressed using a linear approximation of the wire temperature [23], $R_w = R_{ref} [(1 + \alpha (T_w - T_f))]$, where R_{ref} is the baseline resistance of the hot wire and α is the TCR of the graphene. In addition, the heat transfer coefficient (h) can be expressed as the function of fluid velocity (V_f) according to King's law, $h = a + bV_f^c$, where a , b and c are the constants obtained from experimental calibrations. By combining the above equations, one could obtain the relation between the fluidic flow velocity and the temperature gradient of the hot wire, as given by

$$V_f = \left\{ \left[\frac{I^2 R_{ref} [1 + \alpha (T_w - T_{ref})]}{A_w (T_w - T_f)} - a \right] / b \right\}^{1/c}$$

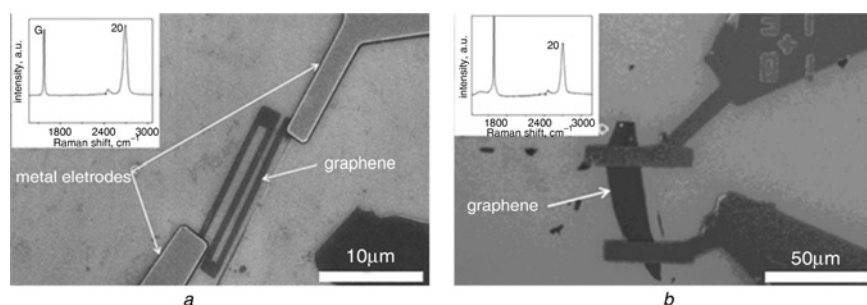


Figure 2 SEM images of the fabricated

a Bi-layer and

b Few-layer graphene hot-wire sensors

The insets show the Raman spectra obtained from the bi-layer and few-layer graphene areas

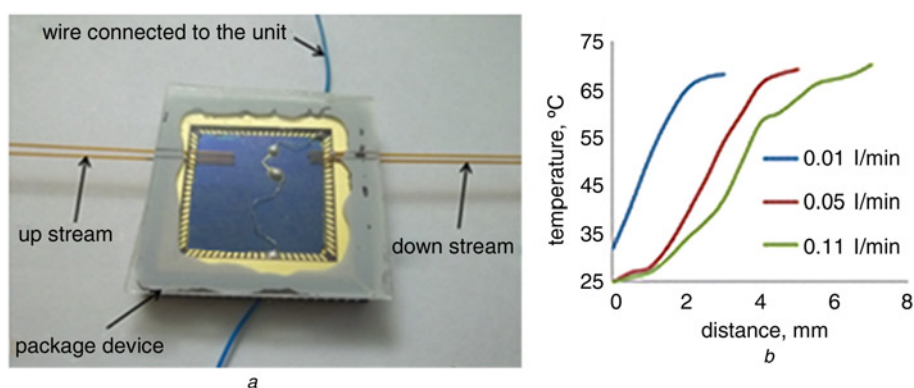


Figure 3 a Device sealed in a DIP carrier with capillaries as upstream and downstream connections

b COMSOL simulation shows the temperature profile of the package against the distance from the inlet at different input flow rates. The carrier was heated at 70°C.

3. Fabrication process: The fabrication process of the proposed graphene hot wires used conventional micro/nanofabrication techniques, as depicted in Fig. 1. Graphene thin films were prepared using a micromechanical exfoliation technique from highly oriented pyrolytic graphite flakes [24] and then transferred onto a 300 nm SiO₂/Si substrate. A microRaman spectroscopy was used to determine the number of layers of the graphene thin films. The mechanical exfoliated bi- and few-layer graphene films were patterned through electronic-beam lithography (EBL) and then an 80 nm copper layer was deposited and patterned as a mask for graphene etching. The graphene area that was not protected by the copper mask was etched in oxygen plasma for 40 s with 150 W radio-frequency (RF) power, 516 mT pressure and 10 sccm flow rate. To dissolve the copper mask, the chip was immersed in a ferric chloride solution for 1 min. After that, conductive electrodes were fabricated on the two terminals of the graphene wire via EBL, thermal evaporation of Ti (5 nm)/Au (75 nm), and then metal lift-off processes. Finally, the devices were annealed in an H₂/Ar environment at 400°C to improve electrode contact resistance and remove fabrication residues. Fig. 2 shows the scanning electron microscopy (SEM) images of the as-fabricated bi- and few-layer graphene hot wires. The bi-layer graphene wire had a length of ~53 μm and the average width of ~0.5 μm. For the few-layer device, the length was about 50 μm and the average width was about 10 μm.

4. Results and discussions: To evaluate their flow sensitivities, the graphene hot wires were placed in a dual inline package (DIP) socket and covered by a glass lid with capillaries (350 μ in outer diameter) as upstream and downstream flow interconnections (Fig. 3a). The gas chamber was sealed with epoxy to minimise

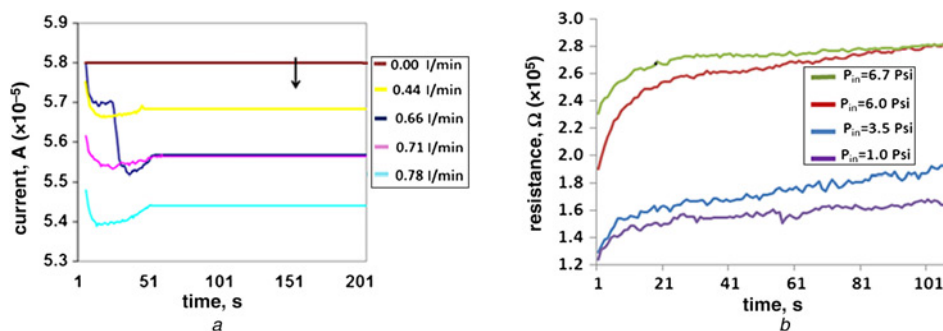


Figure 4 Transient responses of a bi-layer sensor with
a Different N_2 flow rates
b Different N_2 input pressures

side leakage. During the measurement, the temperature of the package was maintained at a constant temperature (70°C) whereas the temperature of nitrogen (N_2) inflow was at room temperature (RT). Prior to flow testing, to determine the proper placement of the graphene sensors, the temperature profile inside the package was simulated with COMSOL Multiphysics 4.3 at different inlet flow rates. As shown in Fig. 3*b*, the temperature varied from 70°C to RT within a narrow range close to the inlet capillary, because of the cooling effect of the N_2 inflow. The simulation result suggests that the sensor should be placed at a particular distance and orientation from the inlet to generate a detectable response. For example, for the flow rate of 0.01 l/min, the sensor should be located less than 2 mm from the inlet capillary tube.

The flow sensing responses of the as-fabricated devices were studied by monitoring the current and resistance changes of the graphene hot wires as the N_2 flow was introduced into the test chamber. Fig. 4 shows the transient responses of a representative bi-layer graphene wire with both various N_2 flow rates and N_2 input pressures. When the gas flowed through the device, the current decreased rapidly with a significant undershoot and then stayed constant with little variation. The steady-state current decreased as the

flow rate increased. The current undershoot could be attributed to the sudden rise of the graphene resistance, which was caused by the temperature drop on the graphene surface, due to the cooling effect of the N_2 flow. As the current continuously passed through the device, the temperature of the graphene wire increased because of current-induced Joule heating, thereby reducing the wire resistance until the equilibrium point was reached for a particular gas flow rate.

Similar testing was performed for the few-layer graphene sensors. Figs. 5*a* and *b* summarise the normalised resistance variations of the bi- and few-layer devices as functions of the N_2 flow rate. The flow sensing resolutions of about 0.07 and 0.1 l/min were obtained from the bi-layer and few-layer graphene hot wires, respectively. Moreover, the negative TCRs of the bi- and few-layer graphene films were determined based on a linear approximation method, resulting in the TCR ranges of -0.00619 to -0.008 K^{-1} for the bi-layer graphene and -0.0014 to -0.00175 K^{-1} for the few-layer graphene. From the histogram of Fig. 5*c*, compared to the mono and few-layer graphene, the bi-layer graphene has the highest negative TCR, measured as the temperature changed between RT and 80°C . Consequently, the

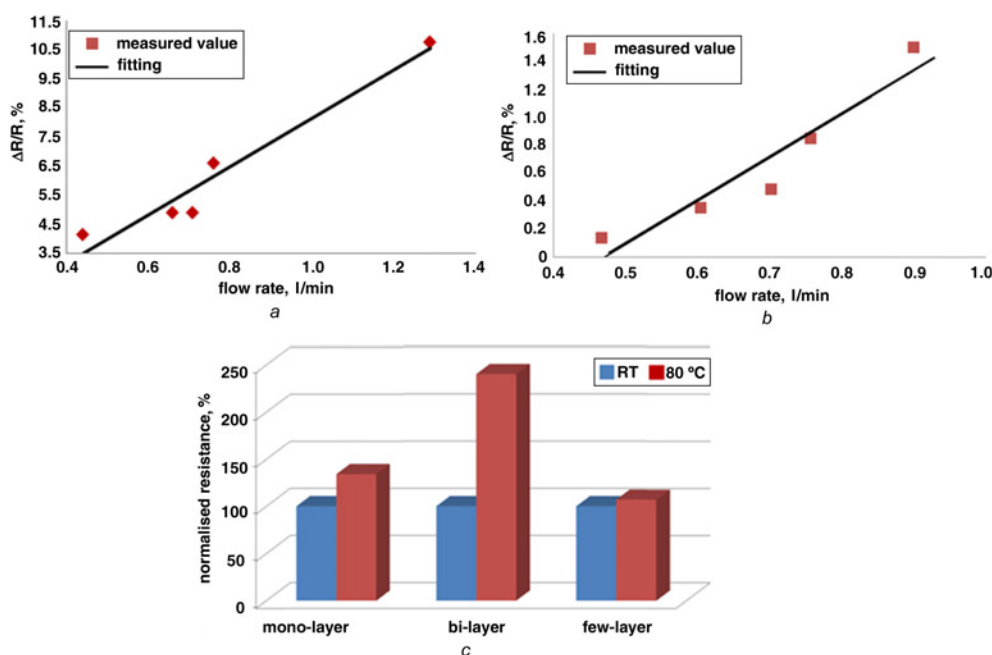


Figure 5 Normalised resistance changes at different flow rates for
a Bi-layer graphene hot wire
b Few-layer sensor
c Resistance changes of the mono-, bi- and few-layer graphene hot wires, measured as the temperature changed between RT and 80°C

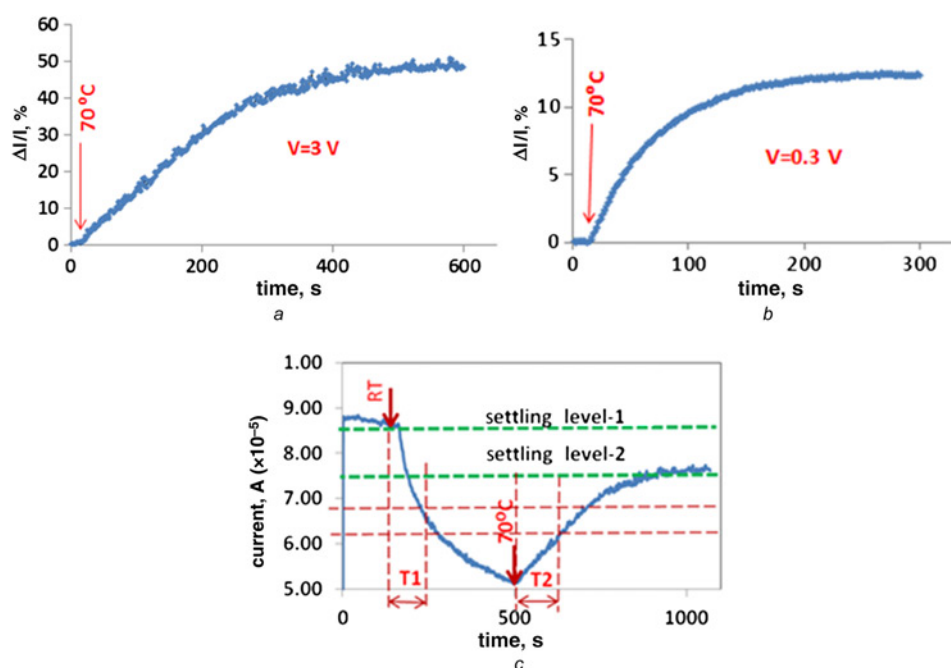


Figure 6 Transient responses of different graphene devices as the environmental temperature varied from RT to 70°C

a Response of a bi-layer graphene sensor

b Response of a few-layer graphene sensor

c Response of the bi-layer device when temperature increased from 70°C to RT and then returned to 70°C

bi-layer device showed a higher current capacity and a higher sensitivity than the mono and few-layer ones.

Time responses to temperature variation for the packaged devices were also measured, as shown in Fig. 6. During the experiment, each device was heated from RT to 70°C and the corresponding current change was monitored as a function of time. It can be found that the device response was faster with a greater applied voltage. For example, for the bi-layer device, the time constant (the time frame when the current reached 63.2% of the steady-state value) was decreased by 18% as the applied voltage increased from 0.5 to 3 V, whereas for the few-layer device the time constant decreased by 40% as the applied voltage increased from 0.1 to 1 V. It is of note that the temperature sensitivity of the bi-layer device was about five times greater than that of the few-layer device, with the applied voltages of 3 and 0.3 V for the bi- and few-layer devices, respectively. Fig. 6c shows the time response of the bi-layer device within a heating-cooling cycle from RT to 70°C and then 70°C to RT. The time constant of the cooling (T_1) step was slightly smaller than the time constant of the heating (T_2) step because the heat source was a hot plate operated in an open environment. The other remarkable thing was that the settling levels of the currents were about 10–20% lower at 70°C than the currents at RT for all the devices. This can be attributed to the variation of the metal-graphene contact resistance with temperature.

Although an increased voltage enhanced the time response of the temperature sensing, the applied voltage was governed by the resistance of the as-fabricated graphene hot wires. This indicates that the device with a lower resistance has a lower allowable applied voltage. Since a high voltage can result in Joule heat to cause imprecise temperature measurement and even device damage, the applied voltage should be properly selected during the sensing applications. Therefore we studied the current-induced self-heating effect in the bi-layer graphene sensor by applying a known voltage across the graphene hot wire and measuring the resulting current change of the device with time. The self-heating can result in the temperature increase of the graphene and lead to the increase in current due to the NTC of the graphene. As shown in Fig. 7, with

an applied voltage of 3 V, the current increased by 20% after – 55 s, as a result of Joule heating.

Based on the experimental results, the heat capacity of the device was extrapolated using $C = ((IV)/(\Delta T)) \times \tau$, where V is the applied voltage, I is the sensor current, τ is the time constant obtained from the graph and ΔT is the temperature gradient because of the power of Joule heating ($P = I \times V$). Since we had two heat sources, Joule heat and a hot plate, it is important to measure the equivalent power of heating at 70°C. To do this, we first measured the graphene resistance at 70°C using the hot plate as the heat source. Then we replaced the hot plate heat with Joule heat and increased the supply voltage of the graphene wire until the same resistance was obtained. The corresponding current (I) and voltage (V) were recorded and the equivalent power (IV) was calculated to determine the heat capacity of the overall system that contained the graphene hotwire, the SiO₂ substrate and the microfluidic carrier. The thermal capacity was $\sim 7.35 \mu\text{Ws}/^\circ\text{C}$ for the bi-layer graphene device with an overall area of $53 \mu\text{m} \times 0.5 \mu\text{m}$ and a supplied voltage of 2.42 V. Since the thermal capacity is one of the significant factors affecting the response time of the

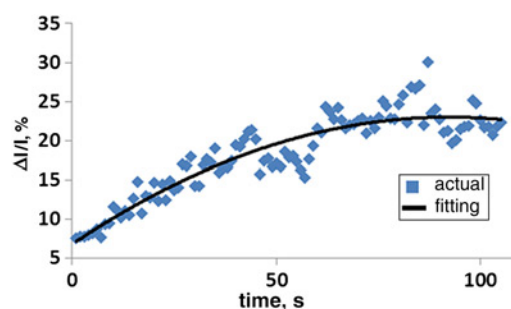


Figure 7 Self-heating effect of a bi-layer graphene device with an applied voltage of 3 V

device, an alternative sensor package with a low thermal capacity and a low thermal mass will further improve the sensor response.

5. Conclusions: In this letter, we studied the surface heat convection properties of the bi- and few-layer graphene wires and used these properties in the development of the flow and temperature sensors. The graphene hot wires were fabricated with specific dimensions to achieve high resistances and uniform temperature distribution. The flow sensing resolutions of ~ 0.07 and 0.1 l/min were achieved from the bi- and few-layer graphene hot wires, respectively. The bi-layer graphene sensor exhibited greater sensitivity than the few layer one because of the larger NTC of the bi-layer graphene. Furthermore, the time response of the current through the graphene hot wires was studied, showing that the time constant decreased as the resistance of the hot wire decreased, because of the reduced Joule heat. For various applications, device design can be tailored to obtain desired sensitivity and time response by optimizing the number of graphene layers, device dimension and applied voltage.

6. Acknowledgments: The authors would like to acknowledge Dr. Baokang Bi, the manager of the clean room in the department of biomedical and physical science at Michigan State University (MSU), for his assistance in the microfabrication. Thanks to Mr. Brian Crum for his help with proofreading the manuscript. The authors thanks also go to Mr. Brian Rook, the research assistant at the Department of Material Science at MSU for his help in the maintenance issues.

7 References

- [1] Johnson R.G., Higashi R.E.: 'A highly sensitive silicon chip micro-transducer for air flow and differential pressure sensing applications', *Sens. Actuators*, 1987, **11**, pp. 63–72
- [2] van Herwaarden A.W., van Duyn D.C., van Oudheusden B.W., Sarro P.M.: 'Integrated thermopile sensors', *Sens. Actuators A, Phys.*, 1989, **22**, pp. 621–630
- [3] Moser D., Lenggenhager R., Baltes H.: 'Silicon gas flow sensors using industrial CMOS and bipolar IC technology', *Sens. Actuators A, Phys.*, 1991, **27**, pp. 577–581
- [4] Hung S.-T., Wong S.-C., Fang W.: 'The development and application of microthermal sensors with a mesh-membrane supporting structure', *Sens. Actuators A, Phys.*, 2000, **84**, pp. 70–75
- [5] Makinwa K.A.A., Huijsing J.H.: 'A smart wind sensor using thermal sigma-delta modulation techniques', *Sens. Actuators A, Phys.*, 2002, **97–98**, pp. 15–20
- [6] Chen J., Fan Z., Zou J., Engel J., Liu C.: 'Two-dimensional micromachined flow sensor array for fluid mechanics studies', *J. Aerosp. Eng.*, 2003, **16**, pp. 85–97
- [7] Sabate N., Santander J., Fonseca L., Gracia I., Cane C.: 'Multi-range silicon micromachined flow sensor', *Sens. Actuators A, Phys.*, 2004, **110**, pp. 282–288
- [8] Svedin N., Kalvesten E., Stemme E., Stemme G.: 'A lift-force flow sensor designed for acceleration insensitivity', *Sens. Actuators A, Phys.*, 1998, **68**, pp. 263–268
- [9] Svedin N., Stemme E., Stemme G.: 'A new bi-directional gas-flow sensor based on lift force'. Proc. 1997 Int. Conf. Solid State Sensors and Actuators, 1997 (TRANSDUCERS '97), Chicago, 1997, vol. **1**, pp. 145–148
- [10] Svedin N., Kalvesten E., Stemme G.: 'A lift force sensor with integrated hot-chips for wide range flow measurements', *Sens. Actuators A, Phys.*, 2003, **109**, pp. 120–130
- [11] Wang Y.-H., Chen C.-P., Chang C.-M., ET AL.: 'MEMS-based gas flow sensors', *Microfluidics Nanofluidics*, 2009, **6**, pp. 333–346
- [12] Su Y., Evans A.G.R., Brunschweiler A., Ensell G.: 'Characterization of a highly sensitive ultra-thin piezoresistive silicon cantilever probe and its application in gas flow velocity sensing', *J. Micromech. Microeng.*, 2002, **12**, pp. 780
- [13] Wang Y.-H., Lee C.-Y., Chiang C.-M.: 'A MEMS-based air flow sensor with a free-standing micro-cantilever structure', *Sensors*, 2007, **7**, pp. 2389–2401
- [14] Geim A.K.: 'Graphene: status and prospects', *Science*, 2009, **324**, pp. 1530–1534
- [15] Chen J.H., Jang C., Xiao S., Ishigami M., Fuhrer M.S.: 'Intrinsic and extrinsic performance limits of graphene devices on SiO₂', *Nature Nanotechnol.*, 2008, **3**, pp. 206–209
- [16] Al-Mumen H., Fubo R., Lixin D., Wen L.: 'Characterization of surface heat convection of bilayer graphene'. Proc. 2012 12th IEEE Conf. Nanotechnology (IEEE-NANO), 2012, pp. 1–4
- [17] Shao Q., Liu G., Teweldebrhan D., Balandin A.A.: 'High-temperature quenching of electrical resistance in graphene interconnects', *Appl. Phys. Lett.*, 2008, **92**, pp. 202108–202108-3
- [18] Fang T., Konar A., Xing H., Jena D.: 'High-field transport in two-dimensional graphene', *Phys. Rev. B*, **84**, pp. 125450
- [19] Alexander A.B.: 'Thermal properties of graphene and nanostructured carbon materials', *Nature Mater.*, 2011, **10**, pp. 569–581
- [20] Skakalova V., Kaiser A.B., Yoo J.S., Oberfell D., Roth S.: 'Correlation between resistance fluctuations and temperature dependence of conductivity in graphene', *Phys. Rev. B*, 2009, **80**, pp. 153404
- [21] Bolotin K.I., Sikes K.J., Hone J., Stormer H.L., Kim P.: 'Temperature-dependent transport in suspended graphene', *Phys. Rev. Lett.*, 2008, **101**, pp. 096802
- [22] Cheianov V.V., Fal'ko V.I.: 'Friedel oscillations, impurity scattering, and temperature dependence of resistivity in graphene', *Phys. Rev. Lett.*, 2006, **97**, pp. 226801
- [23] Bruun H.H.: 'Hot wire anemometry principle and signal analysis' (Oxford Science Publications, 1995, 1st edn.)
- [24] Novoselov K.S., Jiang D., Schedin F., ET AL.: 'Two-dimensional atomic crystals'. Proc. National Academy of Sciences of the United States of America, 26 July 2005, vol. **102**, pp. 10451–10453